A homography-based dynamic control approach of Autonomous Underwater Vehicles observing a (near) vertical target without linear velocity measurements

Lam-Hung Nguyen, Minh-Duc Hua, Tarek Hamel

A homography-based dynamic control approach of Autonomous Underwater Vehicles observing a (near) vertical target without linear velocity measurements

Lam-Hung Nguyen, Minh-Duc Hua and Tarek Hamel

***Abstract*— The paper addresses the challenging problem of image-based dynamic control of Autonomous Underwater Vehicles observing a (near) vertical planar target, without measuring the linear velocity. The proposed control approach exploits a minimum sensor suite consisting of a camera looking forward to provide images from which the homography matrix is extracted and an IMU providing angular velocity and gravity direction measurements. The dynamics of the AUV are exploited in a hierarchical control scheme with inner-outer control loop architecture. Rigourous stability analysis is established. The performance of the proposed approach is illustrated via simulation results conducted on a realistic AUV model.**

I. Introduction

Cameras have been widely used for surveillance and inspection applications involving an Autonomous Underwater Vehicle (AUV). They also provide reliable visual feedback information to control the vehicle's motion. Nowadays, due to the ability of performing high frame rate image processing, monocular cameras are often adopted to perform underwater navigation tasks. When a robotic vehicle operates in an environment containing (near) planar surfaces, the so-called homography [3] that encodes the rotation and scaled translation between two views of a camera observing the same planar target can be used as visual primitive. Homography-based algorithms have been developed over the last 20 years for pose estimation (up to a scale factor) [13], [15], [16]. Proposed by Malis et al. [11], the so-called $2\frac{1}{2}$-D visual servo technique that requires homography decomposition into rotation, scaled translation, and target's normal vector was the foundation of some works in AUV docking [2] and station keeping [10], [17]. A more advanced homography-based visual servoing (HBVS) control scheme is proposed in [1]. The innovative feature is the non-requirement of homography decomposition often computationally expensive [12], making it more relevant for embedded systems. The kinematic control approach developed by [1] has been exploited in our prior work [8] in order to take the full dynamics of fully-actuated AUVs into account, achieving almost global asymptotic stability. The proposed HBVS approach requires, however, linear velocity measurements typically obtained by a Doppler Velocity Log (DVL) that is often unaffordable for low-cost AUVs. Due to such a practical reason, in [14] we have proposed an extension of [8] to the case where linear velocity measurements are not available and the AUV is equipped with a downward-looking camera. The approach has been successfully validated in challenging environments (see `https://bit.ly/2QENdkI` for video demonstration).

We consider here a more challenging case of a fully-actuated AUV equipped with a forward-looking camera observing a (near) vertical visual target. A similar problem concerning underactuated aerial drones has been addressed in [4] which is in line with our effort in dealing with system's dynamics and in depleting the need of a linear velocity sensor. However, that approach relies on the assumption that the *visual velocity* is available for control design, for instance, via the use of a high-gain observer, but a complete stability analysis including such high-gain observer is missing.

This paper is part of our continuing efforts in developing low-cost but efficient visual servoing solutions for AUVs by depleting the need of a costly DVL. Potential applications encompass, for instance, docking on a planar docking station, stabilization or positioning in front of a man-made subsea manifold for performing common tasks in offshore industry such as high-resolution imaging, monitoring, inspection, valve-turning, cleaning, repairing, or changing underwater structures, etc.

This paper is organized as follows. Notation, system modeling and control model are given in Section II. Problem statement is described in Section III. Cascade inner-outer loop control design is presented and analyzed in Section IV. In Section V simulation results on a realistic AUV model are reported, showing the performance of the proposed approach. A concluding section with perspectives then follows.

II. Notation and Modeling

A. Notation

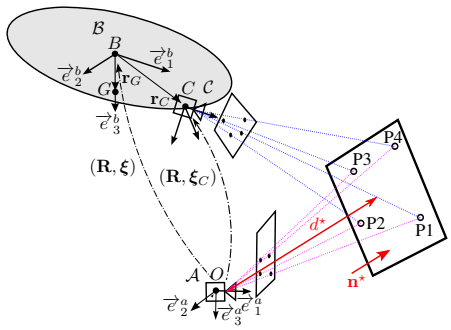

Fig. 1. An AUV with a forward-looking camera and notation

The authors are with I3S laboratory (*Laboratoire d'Informatique, Signaux et Systèmes de Sophia-Antipolis*), CNRS, Université Côte d'Azur, UMR7271, Sophia Antipolis, France. T. Hamel is also with Institut Universitaire de France. Emails: *lhnguyen(hua,thamel)@i3s.unice.fr.*

Let us consider an AUV immersed in water and address the case of absence of current. The following notion is used throughout the paper (see Fig. 1).

• Let m and $\mathbf{J}_0$ denote the vehicle's mass and inertia matrix, G and B its center of mass (CoM) and center of buoyancy (CoB). The distance between G and B is denoted as l. The gravity constant is denoted as g.

• The considered inertial frame is $\mathcal{A} = \{O; \vec{e}^a_1, \vec{e}^a_2, \vec{e}^a_3\}$. The body-fixed frame with the origin at the CoB is denoted as $\mathcal{B} = \{B; \vec{e}^b_1, \vec{e}^b_2, \vec{e}^b_3\}$. The camera frame with base vectors parallel to those of $\mathcal{B}$ is denoted as $\mathcal{C} = \{C; \vec{e}^c_1, \vec{e}^c_2, \vec{e}^c_3\}$. The vectors of coordinates expressed in $\mathcal{B}$ of $\overrightarrow{BC}$ and $\overrightarrow{BG}$ are respectively denoted as $\mathbf{r}_C = [r_{C1}\ r_{C2}\ r_{C3}]^\top \in \mathbb{R}^3$ and $\mathbf{r}_G = l\mathbf{e}_3 \in \mathbb{R}^3$, with $\mathbf{e}_3 = [0\ 0\ 1]^\top$. Denote $\bar{\mathbf{r}}_C = [r_{C1}\ r_{C2}]^\top$.

• The orientation (i.e. attitude) of the frame $\mathcal{B}$ relative to the frame $\mathcal{A}$ is represented by $\mathbf{R} \in \mathrm{SO}(3)$. Let $\boldsymbol{\xi}$ and $\boldsymbol{\xi}_C$ be the vectors of coordinates (expressed in $\mathcal{A}$) of B and C respectively. One has $\boldsymbol{\xi} = \boldsymbol{\xi}_C - \mathbf{R}\mathbf{r}_C$.

• Let $\boldsymbol{\Omega} = [\omega_1\ \omega_2\ \omega_3]^\top \in \mathbb{R}^3$ denote the angular velocity (expressed in $\mathcal{B}$) of $\mathcal{B}$ with respect to $\mathcal{A}$. By denoting $\mathbf{V} = [V_1\ V_2\ V_3]^\top \in \mathbb{R}^3$ and $\mathbf{V}_C = [V_{C1}\ V_{C2}\ V_{C3}]^\top \in \mathbb{R}^3$ respectively the vectors of coordinates (expressed in $\mathcal{B}$) of the linear velocity of B and C, one has $\mathbf{V} = \mathbf{V}_C - \boldsymbol{\Omega} \times \mathbf{r}_C$. Denote $\bar{\mathbf{V}} = [V_1\ V_2]^\top$, $\bar{\mathbf{V}}_C = [V_{C1}\ V_{C2}]^\top$.

• Let $\{\mathbf{e}_1, \mathbf{e}_2, \mathbf{e}_3\}$ denote the canonical basis of $\mathbb{R}^3$ and $\mathbf{I}_n$ denote the identity of $\mathbb{R}^{n\times n}$. For all $\mathbf{u} \in \mathbb{R}^3$, $\mathbf{u}_\times$ denotes the skew-symmetric matrix associated with the cross product by $\mathbf{u}$, i.e., $\mathbf{u}_\times \mathbf{v} = \mathbf{u} \times \mathbf{v}$, $\forall \mathbf{v} \in \mathbb{R}^3$. The Euclidean norm in $\mathbb{R}^n$ and the Frobenius norm in $\mathbb{R}^{n\times n}$ are denoted as $|\cdot|$ and $\|\cdot\|$. Let $\mathrm{sat}^\delta(\cdot) \in \mathbb{R}^n$, with $\delta > 0$, denotes the classical saturation function, i.e., $\mathrm{sat}^\delta(\mathbf{x}) \triangleq \mathbf{x} \min\left(1, \delta/|\mathbf{x}|\right), \forall \mathbf{x} \in \mathbb{R}^n$. Let s_α and c_α denote shortened notations of $\sin(\alpha)$ and $\cos(\alpha)$, $\forall \alpha$.

B. System modeling

The kinematic equations of the AUV are given by

$$\dot{\boldsymbol{\xi}} = \mathbf{R}\mathbf{V} \tag{1a}$$

$$\dot{\mathbf{R}} = \mathbf{R}\boldsymbol{\Omega}_\times \tag{1b}$$

Define the translational and rotational momentums as

$$\begin{cases} \mathbf{P} \triangleq \mathbf{M}\mathbf{V} + \boldsymbol{\Xi}^\top \boldsymbol{\Omega} \\ \boldsymbol{\Pi} \triangleq \mathbf{J}\boldsymbol{\Omega} + \boldsymbol{\Xi}\mathbf{V} \end{cases} \tag{2}$$

with $\mathbf{M} \triangleq m\mathbf{I}_3 + \mathbf{M}_a$, $\mathbf{J} \triangleq \mathbf{J}_0 + \mathbf{J}_a$, $\boldsymbol{\Xi} \triangleq m\mathbf{r}_{G\times}$, and $\mathbf{M}_a$, $\mathbf{J}_a$ denoting the added mass and added inertia matrices respectively. Then, according to the formulation of Leonard [9], the vehicle's dynamics are given by

$$\dot{\mathbf{P}} = \mathbf{P} \times \boldsymbol{\Omega} + \mathbf{F}_c + \mathbf{F}_{gb} + \mathbf{F}_d \tag{3a}$$

$$\dot{\boldsymbol{\Pi}} = \boldsymbol{\Pi} \times \boldsymbol{\Omega} + \mathbf{P} \times \mathbf{V} + \boldsymbol{\Gamma}_c + \boldsymbol{\Gamma}_g + \boldsymbol{\Gamma}_d \tag{3b}$$

where $\mathbf{F}_c \in \mathbb{R}^3$ and $\boldsymbol{\Gamma}_c \in \mathbb{R}^3$ are the control force and torque vertors, $F_{gb} \triangleq mg - F_b$, $\mathbf{F}_{gb} \triangleq F_{gb}\mathbf{R}^\top \mathbf{e}_3$ the sum of the gravity and buoyancy forces, $\boldsymbol{\Gamma}_g \triangleq mg\mathbf{r}_G \times \mathbf{R}^\top \mathbf{e}_3$ the gravity torque, and $\mathbf{F}_d$ and $\boldsymbol{\Gamma}_d$ the damping force and torque modeled as the sum of linear and quadratic terms as follows

$$\begin{cases} \mathbf{F}_d(\mathbf{V}) = -(\mathbf{D}_{Vl} + |\mathbf{V}_h|\mathbf{D}_{Vq})\mathbf{V} \\ \boldsymbol{\Gamma}(\boldsymbol{\Omega}) = -(\mathbf{D}_{\Omega l} + |\boldsymbol{\Omega}|\mathbf{D}_{\Omega q})\boldsymbol{\Omega} \end{cases} \tag{4}$$

with positive damping matrices $\mathbf{D}_{Vl}$, $\mathbf{D}_{Vq}$, $\mathbf{D}_{\Omega l}$, $\mathbf{D}_{\Omega q} \in \mathbb{R}^{3\times 3}$. Note that model (4) of $\mathbf{F}_d$ and $\boldsymbol{\Gamma}_d$ is not used for control design but it is exploited for simulation validations.

C. Model for control design

For simplicity, the added-mass matrix is modeled as a diagonal matrix $\mathbf{M}_a = \mathrm{diag}(m_{a1}, m_{a2}, m_{a3})$. Thus, $\mathbf{M}$ has the form $\mathbf{M} = \mathrm{diag}(m_1, m_2, m_3)$ with $m_i \triangleq m + m_{ai}$ $(i = 1, 2, 3)$. Denote $\bar{\mathbf{M}} \triangleq \mathrm{diag}(m_1, m_2)$.

The translational and rotational dynamics (3a)-(3b) are tightly coupled due to the coupling matrix $\boldsymbol{\Xi}$. This coupling is often neglected in the literature using the fact that the distance between the CoB and CoM is relatively small. Since the linear velocity is not measured, the "Munk moment" $(\mathbf{M}\mathbf{V}) \times \mathbf{V}$ is here considered as a disturbance. Finally, the damping force and torque are also considered as disturbances. These considerations result in the following simpler dynamic equations that decouple the translational and rotational dynamics:

$$\mathbf{M}\dot{\mathbf{V}} = (\mathbf{M}\mathbf{V}) \times \boldsymbol{\Omega} + \mathbf{F}_c + \mathbf{F}_{gb} + \boldsymbol{\Delta}_F \tag{5a}$$

$$\mathbf{J}\dot{\boldsymbol{\Omega}} = (\mathbf{J}\boldsymbol{\Omega}) \times \boldsymbol{\Omega} + \boldsymbol{\Gamma}_c + \boldsymbol{\Gamma}_g + \boldsymbol{\Delta}_\Gamma \tag{5b}$$

with the "disturbance" terms

$$\boldsymbol{\Delta}_F \triangleq (\boldsymbol{\Xi}^\top \boldsymbol{\Omega})_\times \boldsymbol{\Omega} - \boldsymbol{\Xi}^\top \dot{\boldsymbol{\Omega}} + \mathbf{F}_d$$
$$\boldsymbol{\Delta}_\Gamma \triangleq (\boldsymbol{\Xi}\mathbf{V}) \times \boldsymbol{\Omega} + \mathbf{P} \times \mathbf{V} - \boldsymbol{\Xi}\dot{\mathbf{V}} + \boldsymbol{\Gamma}_d$$

In absence of current the term $\boldsymbol{\Delta}_F$ would eventually converge to zero in fixed-point stabilization problem. Since $\mathbf{F}_d$ is a dissipative force, it is reasonable to neglect $\boldsymbol{\Delta}_F$ in control design (i.e. setting $\boldsymbol{\Delta}_F \equiv \mathbf{0}$).

III. Problem Formulation

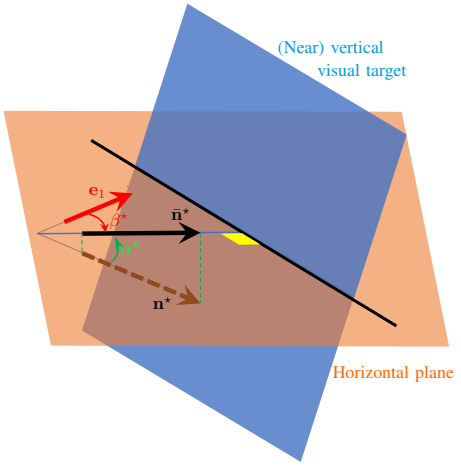

Fig. 2. Illustration of angles $\alpha^\star$ and $\beta^\star$. The projection vector $\bar{\mathbf{n}}^\star$ and $\mathbf{e}_1$ lie on the horizontal plane and $\bar{\mathbf{n}}^\star$ is perpendicular to the intersection line of the two planes.

Based on a reference image, taken at some desired pose using a forward-looking monocular camera, and the current images, the control design objective consists in stabilizing the camera's pose to the reference one. Let us choose the inertial frame $\mathcal{A}$ attached to the camera's desired pose (see Fig. 1). Assume that a good estimate of the homography matrix $\mathbf{H}$ is available for control design. This latter encodes geometric

information about the rotation and translation between the current camera frame $\mathcal{C}$ and the reference frame $\mathcal{A}$ [1]

$$\begin{bmatrix} h_{11} & h_{12} & h_{13} \\ h_{21} & h_{22} & h_{23} \\ h_{31} & h_{32} & h_{33} \end{bmatrix} \triangleq \mathbf{H} = \mathbf{R}^\top (\mathbf{I}_3 - \frac{1}{d^\star} \boldsymbol{\xi}_C \mathbf{n}^{\star\top}) \quad (6)$$

with $d^\star$ the distance between the camera optical center and the target plane and $\mathbf{n}^\star \in S^2$ the unit vector normal pointing towards the target plane expressed in $\mathcal{A}$ (see Fig. 1).

Denote $\bar{\mathbf{n}}^\star$ the projection vector of $\mathbf{n}^\star$ on the horizontal plane; $\beta^\star$ the angle between $\bar{\mathbf{n}}^\star$ and camera optical axis when taking the reference image; and $\alpha^\star$ the angle between $\mathbf{n}^\star$ and the horizontal plane (see Fig. 2). One verifies that

$$\mathbf{n} = [n_1 \; n_2 \; n_3]^\top \triangleq \frac{\mathbf{n}^\star}{d^\star} = \frac{1}{d^\star} \begin{bmatrix} c_{\alpha^\star} c_{\beta^\star} & c_{\alpha^\star} s_{\beta^\star} & s_{\alpha^\star} \end{bmatrix}^\top \quad (7)$$

Since the visual target is within the camera's field of view (FOV) when taking the reference image, one should have $|\alpha^\star|, |\beta^\star| < \frac{\pi}{2}$, which in turn imply that $n_1 > 0$.

In addition to the estimation of $\mathbf{H}$, it is assumed that an Inertial Measurement Unit (IMU) is available to provide measurements of the angular velocity $\boldsymbol{\Omega}$ together with an approximate of the gravity direction $\mathbf{R}^\top \mathbf{e}_3$.

The control objective consists in stabilizing $\mathbf{H}$ about $\mathbf{I}_3$ (or equivalently stabilizing $(\mathbf{R}, \boldsymbol{\xi}_C)$ about $(\mathbf{I}_3, \mathbf{0})$) using only $(\mathbf{H}, \boldsymbol{\Omega}, \mathbf{R}^\top \mathbf{e}_3)$ as available information. In addition to the lack of the linear velocity measurement, the main issues of control design are retated to the unknown terms $d^\star$ and $\mathbf{n}^\star$ involved in the expression (6) of $\mathbf{H}$. More importantly, we here exploit directly $\mathbf{H}$ without extracting the usual components $(\mathbf{R}, \frac{\boldsymbol{\xi}_C}{d^\star}, \mathbf{n}^\star)$ via a complex and computationally expensive decomposition [12].

IV. Control Design

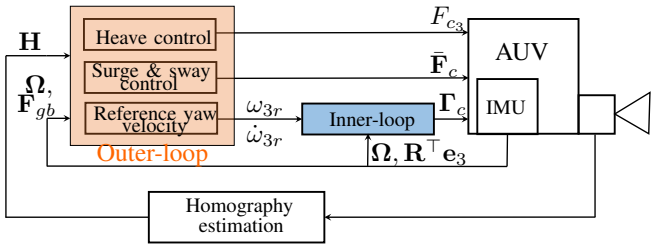

Fig. 3. Control architecture of the proposed HBVS

A cascade inner-outer loop control architecture as depicted in Fig. 3 is proposed.

- The inner-loop controller (developed in Subsection IV-B) governs the rotation dynamics (1b) and (5b) by defining the torque control vector $\boldsymbol{\Gamma}_c$ to ensure the almost global asymptotic stability (almost-GAS) of the equilibrium $(\boldsymbol{\Omega}, \mathbf{R}^\top \mathbf{e}_3) = (\boldsymbol{\Omega}_r, \mathbf{e}_3)$, where the reference angular velocity $\boldsymbol{\Omega}_r$ is defined by

$$\boldsymbol{\Omega}_r \triangleq k_g \mathbf{e}_3 \times \mathbf{R}^\top \mathbf{e}_3 + \omega_{3r} \mathbf{e}_3 \quad (8)$$

  with $k_g > 0$ positive gain and $\omega_{3r} \in \mathbb{R}$ the reference yaw angular velocity to be specified by the outer-loop controller. Assume that ω_{3r} is bounded by design. Note that $\dot{\omega}_{3r}$ must be computable so that the feedforward term $\dot{\boldsymbol{\Omega}}_r$ is also computable by the torque controller.
- The outer-loop controller (developed in Subsection IV-A) defines the force control vector $\mathbf{F}_c$ and the reference yaw angular velocity ω_{3r} (used by the inner-loop controller) to fulfill the main objective of stabilizing $(\mathbf{R}, \boldsymbol{\xi}_C)$ about $(\mathbf{I}_3, \mathbf{0})$.

In the sequel we first present the outer-loop control design, which constitutes the main contribution of this paper. The design for the inner-loop is less involved and is postponed after the outer-loop control design.

A. Outer-loop control design

Let ψ denote the AUV's yaw angle and $\mathbf{R}_\psi$ the rotation matrix around AUV's axis $\overrightarrow{e}_3^b$. Denote

$$\boldsymbol{\Delta}_R = \begin{bmatrix} \Delta_{11} & \Delta_{12} & \Delta_{13} \\ \Delta_{21} & \Delta_{22} & \Delta_{23} \\ \Delta_{31} & \Delta_{32} & \Delta_{33} \end{bmatrix} \triangleq \mathbf{R}^\top - \mathbf{R}_\psi^\top$$

Since $\mathbf{R}^\top \mathbf{e}_3$ converge to $\mathbf{e}_3$ as a result of the inner-loop controller, one verifies that $\boldsymbol{\Delta}_R$ converges to zero. The convergence of $\mathbf{R}^\top \mathbf{e}_3$ about $\mathbf{e}_3$ implies that ω_1 and ω_2 converge to zero. One then deduces that $\dot{\boldsymbol{\Delta}}_R$ remains bounded and converges to zero.

Define the following visual errors

$$\boldsymbol{\sigma} \triangleq \begin{bmatrix} -h_{11} + h_{22} \\ -h_{12} - h_{21} \end{bmatrix}, \quad \varrho \triangleq -h_{31}$$

Using (6) one deduces

$$\begin{bmatrix} \boldsymbol{\sigma} \\ \varrho \end{bmatrix} = \begin{bmatrix} \mathbf{N} & 0 \\ 0 & n_1 \end{bmatrix} \mathbf{R}^\top \boldsymbol{\xi}_C + \begin{bmatrix} -\Delta_{11} + \Delta_{22} \\ -\Delta_{12} - \Delta_{21} \\ -\Delta_{31} \end{bmatrix} \quad (9)$$

with $\mathbf{N} \triangleq n_1 \mathbf{I}_2 + n_2 \mathbf{S}$, $\mathbf{S} \triangleq \begin{bmatrix} 0 & -1 \\ 1 & 0 \end{bmatrix}$. This in turn yields

$$\mathbf{R}^\top \boldsymbol{\xi}_C = \begin{bmatrix} \mathbf{N}^{-1} & 0 \\ 0 & \frac{1}{n_1} \end{bmatrix} \begin{bmatrix} \boldsymbol{\sigma} \\ \varrho \end{bmatrix} - \begin{bmatrix} \mathbf{N}^{-1} & 0 \\ 0 & \frac{1}{n_1} \end{bmatrix} \begin{bmatrix} -\Delta_{11} + \Delta_{22} \\ -\Delta_{12} - \Delta_{21} \\ -\Delta_{31} \end{bmatrix} \quad (10)$$

Using (9) and (10) one verifies that

$$\begin{aligned} \dot{\boldsymbol{\sigma}} = & -\omega_3 \mathbf{S} \boldsymbol{\sigma} + \mathbf{N} \bar{\mathbf{V}}_C - \frac{\varrho}{n_1} \mathbf{N} \boldsymbol{\omega}_{12} - \frac{\Delta_{31}}{n_1} \mathbf{N} \boldsymbol{\omega}_{12} \\ & + \omega_3 \mathbf{S} \begin{bmatrix} -\Delta_{11} + \Delta_{22} \\ -\Delta_{12} - \Delta_{21} \end{bmatrix} + \begin{bmatrix} -\dot{\Delta}_{11} + \dot{\Delta}_{22} \\ -\dot{\Delta}_{12} - \dot{\Delta}_{21} \end{bmatrix} \end{aligned} \quad (11)$$

$$\begin{aligned} \dot{\varrho} = & \; n_1 V_3 + n_1 \boldsymbol{\omega}_{12}^\top \mathbf{N}^{-1} \boldsymbol{\sigma} \\ & - n_1 \boldsymbol{\omega}_{12}^\top \mathbf{N}^{-1} \begin{bmatrix} -\Delta_{11} + \Delta_{22} \\ -\Delta_{12} - \Delta_{21} \end{bmatrix} - \dot{\Delta}_{31} \end{aligned} \quad (12)$$

with $\boldsymbol{\omega}_{12} \triangleq \begin{bmatrix} \omega_2 & -\omega_1 \end{bmatrix}^\top$. By denoting $\bar{\mathbf{P}} \triangleq [P_1 \; P_2]^\top$ (respectively $\bar{\mathbf{F}}_c \triangleq [F_{c1} \; F_{c2}]^\top$), the vector of the two first components of $\mathbf{P}$ (respectively $\mathbf{F}_c$), and rewriting $\mathbf{F}_{gb} = F_{gb} \begin{bmatrix} \Delta_{13} & \Delta_{23} & 1 + \Delta_{33} \end{bmatrix}^\top$, one can write (5a) as two interconnected dynamics (surge-and-sway and heave) as follows

$$\dot{\bar{\mathbf{P}}} = -\omega_3 \mathbf{S} \bar{\mathbf{P}} + \bar{\mathbf{F}}_c - \boldsymbol{\omega}_{12} P_3 + F_{gb} \begin{bmatrix} \Delta_{13} \\ \Delta_{23} \end{bmatrix} \quad (13a)$$

$$\dot{P}_3 = F_{c3} + F_{gb} + \boldsymbol{\omega}_{12}^\top \bar{\mathbf{P}} + F_{gb} \Delta_{33} \quad (13b)$$

with P_3 the third component of $\mathbf{P}$. Introduce a new velocity

variable[1]

$$\bar{\bar{\mathbf{V}}} \triangleq \bar{\mathbf{V}} + \omega_{3r}\mathbf{S}\bar{\mathbf{r}}_C \tag{14}$$

One verifies that

$$\bar{\mathbf{V}}_C = \bar{\bar{\mathbf{V}}} + (\omega_3 - \omega_{3r})\mathbf{S}\bar{\mathbf{r}}_C + r_{C3}\boldsymbol{\omega}_{12} \tag{15}$$

Define the following new control force

$$\bar{\bar{\mathbf{F}}}_c \triangleq \bar{\mathbf{F}}_c + \left(\dot{\omega}_{3r}\mathbf{I}_2 + \omega_{3r}^2\mathbf{S}\right)\bar{\mathbf{M}}\mathbf{S}\bar{\mathbf{r}}_C \tag{16}$$

Denoting $\bar{\bar{\mathbf{P}}} \triangleq \bar{\mathbf{M}}\bar{\bar{\mathbf{V}}}$ and using (14), (15), (16), Subsystem (11)+ (13a) and Subsystem (12)+(13b) can be rewritten as

$$\begin{cases} \dot{\boldsymbol{\sigma}} = -\omega_3\mathbf{S}\boldsymbol{\sigma} + \mathbf{N}\bar{\mathbf{M}}^{-1}\bar{\bar{\mathbf{P}}} - \dfrac{\varrho}{n_1}\mathbf{N}\boldsymbol{\omega}_{12} + \boldsymbol{\varepsilon}_1 \\ \dot{\bar{\bar{\mathbf{P}}}} = -\omega_3\mathbf{S}\bar{\bar{\mathbf{P}}} + \bar{\bar{\mathbf{F}}}_c - P_3\boldsymbol{\omega}_{12} + \boldsymbol{\varepsilon}_2 \end{cases} \tag{17}$$

$$\begin{cases} \dot{\varrho} \;\; = \frac{n_1}{m_3}P_3 + n_1\boldsymbol{\omega}_{12}^\top\mathbf{N}^{-1}\boldsymbol{\sigma} + \varepsilon_3 \\ \dot{P}_3 = F_{c3} + F_{gb} + \boldsymbol{\omega}_{12}^\top\bar{\bar{\mathbf{P}}} + \varepsilon_4 \end{cases} \tag{18}$$

with bounded vanishing terms

$$\begin{cases} \boldsymbol{\varepsilon}_1 \triangleq (\omega_3 - \omega_{3r})\mathbf{N}\mathbf{S}\bar{\mathbf{r}}_C + r_{C3}\mathbf{N}\boldsymbol{\omega}_{12} - \dfrac{\Delta_{31}}{n_1}\mathbf{N}\boldsymbol{\omega}_{12} \\ \qquad + \omega_3\mathbf{S}\begin{bmatrix} -\Delta_{11} + \Delta_{22} \\ -\Delta_{12} - \Delta_{21} \end{bmatrix} + \begin{bmatrix} -\dot{\Delta}_{11} + \dot{\Delta}_{22} \\ -\dot{\Delta}_{12} - \dot{\Delta}_{21} \end{bmatrix} \\ \boldsymbol{\varepsilon}_2 \triangleq F_{gb}\begin{bmatrix} \Delta_{13} \\ \Delta_{23} \end{bmatrix} \\ \varepsilon_3 \triangleq -\dot{\Delta}_{31} - n_1\boldsymbol{\omega}_{12}^\top\mathbf{N}^{-1}\begin{bmatrix} -\Delta_{11} + \Delta_{22} \\ -\Delta_{12} - \Delta_{21} \end{bmatrix} \\ \varepsilon_4 \triangleq -\omega_{3r}\boldsymbol{\omega}_{12}^\top\bar{\mathbf{M}}\mathbf{S}\bar{\mathbf{r}}_C + F_{gb}\Delta_{33} \end{cases}$$

One observes that systems (17) and (18) are interconnected (see Fig. 4). In the sequel we first neglect all coupling terms in the outer-loop control design. This is intuitively guided by the fact that these terms are multiplicative terms by vanishing variables ω_1 and ω_2. Then, a more complete stability analysis for this interconnected system will be carried out thereafter.

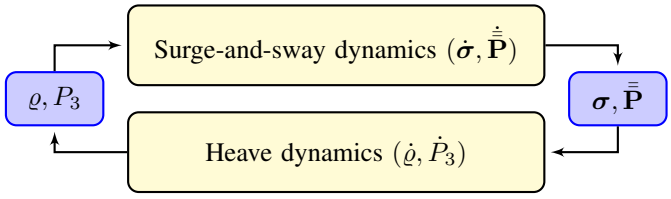

Fig. 4. Interconnected translational dynamics

1) Heave control design: Similarly to the approach proposed in [14], the altitude (heave) control can be designed independently from surge-and-sway and yaw control design.

Proposition 1 *Consider System* (18) *where the coupling terms involving* $\boldsymbol{\sigma}$ *and* $\bar{\bar{\mathbf{P}}}$ *are neglected. Introduce the augmented system*

$$\dot{\hat{\varrho}} = -k_{13}(\hat{\varrho} - \varrho), \;\; \hat{\varrho}(0) = \varrho(0)$$

with $k_{13} > 0$. *Apply the control force*

$$F_{c3} = m_3k_{23}\hat{\varrho} - m_3k_{33}\varrho - (mg - F_b)$$

[1] $\bar{\bar{V}}$ is used for handling the case with an arbitrary position of the camera w.r.t the COB. The convergence of ω_{3r} to zero then results in $\bar{V} \to \bar{\bar{V}}$.

with $k_{33} > k_{23} > 0$. *Then, the equilibrium* $(\hat{\varrho}, \varrho, P_3) = (0, 0, 0)$ *of the controlled system is globally asymptotically stable (GAS) with exponential convergence rate after some time instant* $T > 0$.

Proof: The considered system can be rewritten as

$$\dot{\mathbf{x}} = \bar{\mathbf{A}}\mathbf{x} + \boldsymbol{\varepsilon}_{34} \tag{19}$$

with

$$\mathbf{x} \triangleq \begin{bmatrix} \hat{\varrho} \\ \varrho \\ P_3 \end{bmatrix}, \; \bar{\mathbf{A}} \triangleq \begin{bmatrix} -k_{13} & k_{13} & 0 \\ 0 & 0 & \frac{n_1}{m_3} \\ m_3k_{23} & -m_3k_{33} & 0 \end{bmatrix}, \; \boldsymbol{\varepsilon}_{34} \triangleq \begin{bmatrix} 0 \\ \varepsilon_3 \\ \varepsilon_4 \end{bmatrix} \tag{20}$$

From there, the proof is straightforward since the nominal system $\dot{\mathbf{x}} = \bar{\mathbf{A}}\mathbf{x}$ is Hurwitz (using $k_{33} > k_{23} > 0$) while the perturbation terms ε_3 and ε_4 converge to zero. ■

2) Surge-and-sway control design: Consider System (17) and neglect all coupling terms involving ϱ and P_3. Introduce the following augmented system

$$\dot{\hat{\boldsymbol{\sigma}}} = -\omega_3\mathbf{S}\hat{\boldsymbol{\sigma}} - k_1\hat{\boldsymbol{\sigma}} + k_1\boldsymbol{\sigma}, \quad \hat{\boldsymbol{\sigma}}(0) = \boldsymbol{\sigma}(0) \tag{21}$$

with $k_1 > 0$. Apply the control force

$$\bar{\bar{\mathbf{F}}}_c = k_2\bar{\mathbf{M}}\hat{\boldsymbol{\sigma}} - k_3\bar{\mathbf{M}}\boldsymbol{\sigma} \tag{22}$$

with $k_2, k_3 > 0$. Then, the controlled surge-and-sway subsystem is given by

$$\begin{cases} \dot{\hat{\boldsymbol{\sigma}}} = -\omega_3\mathbf{S}\hat{\boldsymbol{\sigma}} - k_1\hat{\boldsymbol{\sigma}} + k_1\boldsymbol{\sigma} \\ \dot{\boldsymbol{\sigma}} = -\omega_3\mathbf{S}\boldsymbol{\sigma} + \mathbf{N}\bar{\mathbf{M}}^{-1}\bar{\bar{\mathbf{P}}} + \boldsymbol{\varepsilon}_1 \\ \dot{\bar{\bar{\mathbf{P}}}} = -\omega_3\mathbf{S}\bar{\bar{\mathbf{P}}} + k_2\bar{\mathbf{M}}\hat{\boldsymbol{\sigma}} - k_3\bar{\mathbf{M}}\boldsymbol{\sigma} + \boldsymbol{\varepsilon}_2 \end{cases} \tag{23}$$

Denote

$$\mathbf{X}_1 = \begin{bmatrix} x_{11} \\ x_{12} \end{bmatrix} \triangleq \hat{\boldsymbol{\sigma}}, \;\; \mathbf{X}_2 = \begin{bmatrix} x_{21} \\ x_{22} \end{bmatrix} \triangleq \boldsymbol{\sigma}, \;\; \mathbf{X}_3 = \begin{bmatrix} x_{31} \\ x_{32} \end{bmatrix} \triangleq \bar{\bar{\mathbf{P}}}$$

$$\mathbf{X} \triangleq \begin{bmatrix} \mathbf{X}_1 \\ \mathbf{X}_2 \\ \mathbf{X}_3 \end{bmatrix}, \; \boldsymbol{\varepsilon}_{12} \triangleq \begin{bmatrix} \mathbf{0} \\ \boldsymbol{\varepsilon}_1 \\ \boldsymbol{\varepsilon}_2 \end{bmatrix}, \; \bar{\mathbf{S}} \triangleq \begin{bmatrix} \mathbf{S} & 0 & 0 \\ 0 & \mathbf{S} & 0 \\ 0 & 0 & \mathbf{S} \end{bmatrix} \tag{24}$$

$$\mathbf{A} \triangleq \begin{bmatrix} -k_1\mathbf{I}_2 & k_1\mathbf{I}_2 & 0 \\ 0 & 0 & n_1\bar{\mathbf{M}}^{-1} \\ k_2\bar{\mathbf{M}} & -k_3\bar{\mathbf{M}} & 0 \end{bmatrix}, \mathbf{B} \triangleq \begin{bmatrix} 0 & 0 & 0 \\ 0 & 0 & n_2\mathbf{S}\bar{\mathbf{M}}^{-1} \\ 0 & 0 & 0 \end{bmatrix} \tag{25}$$

System (23) can be rewritten as

$$\dot{\mathbf{X}} = -\omega_{3r}\bar{\mathbf{S}}\mathbf{X} + \mathbf{A}\mathbf{X} + \mathbf{B}\mathbf{X} - \tilde{\omega}_3\bar{\mathbf{S}}\mathbf{X} + \boldsymbol{\varepsilon}_{12} \tag{26}$$

with $\tilde{\omega}_3 \triangleq \omega_3 - \omega_{3r}$. In the sequel we will specify a sufficient condition ensuring that the origin of System (26) is GAS.

Lemma 1 *Consider system*

$$\dot{\mathbf{X}} = \mathbf{A}\mathbf{X} + \mathbf{B}\mathbf{X} \tag{27}$$

with $\mathbf{A}$ *and* $\mathbf{B}$ *defined in* (25). *Assume that the reference image is captured with a reference heading angle satisfying*

$$|\beta^\star| < \beta^\star_{max} \triangleq \arctan\left(\frac{1}{\sqrt{1+\sqrt{2}}}\right) \approx 32.8^\circ \tag{28}$$

Then, there exist $\bar{k}_1 > 0$ *large and* $\epsilon > 0$ *small enough, with* $\bar{k}_1$ *and* ϵ *depending on* $(\beta^\star_{max}, |\beta^\star|)$, *such that system* (27) *is globally exponentially stable (GES) provided that* $k_1 > \bar{k}_1$, $1 < k_3/k_2 < 1 + \epsilon$.

The proof is given in Appendix I.

Proposition 2 *Consider System* (26)*. Assume that all assumptions of Lemma 1 hold. Assume that the inner-loop controller ensures the uniform boundedness and convergence to zero of $\boldsymbol{\varepsilon}_{12}$ and $\tilde{\omega}_3$. Then, there exists a positive number ϖ such that if $\sup|\omega_{3r}| < \varpi$ then the equilibrium $\mathbf{X} = \mathbf{0}$ is GAS with exponential convergence rate after some time instant $T > 0$.*

The proof is given in Appendix II.

So far the outer-loop control design and associated stability analysis have been carried out for systems (17) and (18) by neglecting all coupling terms. Next, stability analysis for the full interconnected system will be developed. The interconnected system (17)–(18) can be rewritten as

$$\begin{cases} \dot{\mathbf{X}} = -\omega_3(t)\bar{\mathbf{S}}\mathbf{X} + \mathbf{A}\mathbf{X} + \mathbf{B}\mathbf{X} + \mathbf{E}_1\mathbf{x} + \boldsymbol{\varepsilon}_{12} \\ \dot{\mathbf{x}} = \bar{\mathbf{A}}\mathbf{x} + \mathbf{E}_2\mathbf{X} + \boldsymbol{\varepsilon}_{34} \end{cases} \tag{29}$$

with vanishing matrices

$$\mathbf{E}_1 \triangleq \begin{bmatrix} \mathbf{0} & \mathbf{0} & \mathbf{0} \\ \mathbf{0} & -\frac{\mathbf{N}}{n_1}\boldsymbol{\omega}_{12} & \mathbf{0} \\ \mathbf{0} & \mathbf{0} & -\boldsymbol{\omega}_{12} \end{bmatrix}, \mathbf{E}_2 \triangleq \begin{bmatrix} \mathbf{0} & \mathbf{0} & \mathbf{0} \\ \mathbf{0} & n_1\boldsymbol{\omega}_{12}^\top\mathbf{N}^{-1} & \mathbf{0} \\ \mathbf{0} & \mathbf{0} & \boldsymbol{\omega}_{12}^\top \end{bmatrix} \tag{30}$$

Theorem 1 *Consider the interconnected system* (29)*. Assume that all assumptions in Propositions 1 and 2 hold. Assume that all outer-loop control gains and ω_{3r} are chosen as in Propositions 1 and 2. Assume that the inner-loop controller ensures the uniform boundedness and convergence to zero of $\boldsymbol{\varepsilon}_{12}$, $\boldsymbol{\varepsilon}_{34}$ and $\tilde{\omega}_3$. Then, the equilibrium $(\mathbf{X}, \mathbf{x}) = (\mathbf{0}, \mathbf{0})$ is GAS with exponential convergence rate after some time instant.*

Proof: As a result of Propositions 1 and 2, there exists a time instant $T_1 > 0$ and some positive numbers α_1, α_2, β_1, β_2 such that $\forall t \geq T_1$ one has

$$\begin{aligned} \frac{\mathrm{d}}{\mathrm{d}t}(\mathbf{X}^\top\mathbf{D}\mathbf{X}) &\leq -\alpha_1|\mathbf{X}|^2 + \beta_1\|\mathbf{E}_1\|\,|\mathbf{X}|\,|\mathbf{x}| \\ \frac{\mathrm{d}}{\mathrm{d}t}(\mathbf{x}^\top\bar{\mathbf{D}}\mathbf{x}) &\leq -\alpha_2|\mathbf{x}|^2 + \beta_2\|\mathbf{E}_2\|\,|\mathbf{X}|\,|\mathbf{x}| \end{aligned}$$

with $\mathbf{D}$ given in the proof of Lemma 1 and $\bar{\mathbf{D}}$ the symmetric positive matrix solution to the Lyapunov equation $\bar{\mathbf{D}}\bar{\mathbf{A}} + \bar{\mathbf{A}}^\top\bar{\mathbf{D}} = -\mathbf{I}_3$. Subsequently, the time-derivative of the aggregate Lyapunov function $\mathcal{L} \triangleq \mathbf{X}^\top\mathbf{D}\mathbf{X} + \mathbf{x}^\top\bar{\mathbf{D}}\mathbf{x}$ satisfies

$$\dot{\mathcal{L}}(t \geq T_1) \leq -\alpha_1|\mathbf{X}|^2 - \alpha_2|\mathbf{x}|^2 + (\beta_1\|\mathbf{E}_1\| + \beta_2\|\mathbf{E}_2\|)|\mathbf{X}|\,|\mathbf{x}|$$

Since $\mathbf{E}_1$ and $\mathbf{E}_2$ converge uniformly to zero, there exists another time instant $T_2 > T_1$ such that $\forall t \geq T_2$ the cross term is dominated by the quadratic terms. Thus, there exists a positive number ν such that $\dot{\mathcal{L}}(t \geq T_2) \leq -\nu\mathcal{L}(t \geq T_2)$, implying the exponential convergence of $(\mathbf{X}, \mathbf{x})$ to zero. ■

3) Control design of the reference yaw angular velocity ω_{3r}: The previous parts of outer-loop control design ensure the convergence of $\boldsymbol{\xi}_C$ to zero. In view of the definition (6) of the homography, $\mathbf{H}$ converges to $\mathbf{R}^\top$, which in turn converges to $\mathbf{R}_\psi^\top$ as a consequence of the inner-loop controller. Therefore, the component h_{12} of $\mathbf{H}$ converges to $\sin\psi$. It, thus, can be exploited for the design of ω_{3r} for ensuring the convergence of $\mathbf{R}$ to $\mathbf{I}$. Note that the whole control design process in the previous subsections is based on the assumption about the boundedness of ω_{3r} (see Proposition 2). The design of ω_{3r} and associated stability analysis (omitted due to space limitation) proceeds identically to our prior work [6].

Proposition 3 *Assume that the inner-loop torque control $\boldsymbol{\Gamma}_c$ ensures the almost-GAS of the equilibrium $(\boldsymbol{\Omega}, \mathbf{R}^\top\mathbf{e}_3) = (\boldsymbol{\Omega}_r, \mathbf{e}_3)$, with $\boldsymbol{\Omega}_r$ defined by* (8) *combined with ω_{3r} (involved in* (8)*) solution to the following system*

$$\dot{\omega}_{3r} = -k_{\Theta 2}\omega_{3r} - k_{\Theta 1}\mathrm{sat}^{\Delta_\Theta}(h_{12}), \quad \omega_{3r}(0) \in \mathbb{R} \tag{31}$$

with positive numbers $k_{\Theta 1}, k_{\Theta 2}, \Delta_\Theta$ satisfying $\frac{k_{\theta_1}}{k_{\theta_2}}\Delta_\Theta < \varpi$ where ϖ is defined from Proposition 2. Apply the outer-loop force control $\mathbf{F}_c = \begin{bmatrix} \bar{\mathbf{F}}_c^\top & F_{c_3} \end{bmatrix}^\top$ where $\bar{\mathbf{F}}_c$ is given by (16)+(22) *with control gains k_2, k_3 specified in Lemma 1 and F_{c3} is defined in Proposition 1. Then, the equilibrium $(\mathbf{R}, \boldsymbol{\xi}_C) = (\mathbf{I}_3, \mathbf{0})$ is almost-GAS.*

B. Inner-loop control design

The more involved part concerning the outer-loop control design has been presented. The design of an effective inner-loop torque controller that ensures the stability of the equilibrium $(\boldsymbol{\Omega}, \mathbf{R}^\top\mathbf{e}_3) = (\boldsymbol{\Omega}_r, \mathbf{e}_3)$, with $\boldsymbol{\Omega}_r$ defined by (8) combined with (31) proceeds identically to our prior work [14] and is, thus, recalled for the sake of completeness.

In view of the rotation dynamics (i.e. (1b) and (5b)), it is not too difficult to carry out the above-mentioned objective since the sub-system under consideration is fully-actuated and the measurements of both $\boldsymbol{\Omega}$ and $\mathbf{R}^\top\mathbf{e}_3$ are at our disposal. Remark that the disturbance term $\boldsymbol{\Delta}_\Gamma$, which containing the Munk moment $\mathbf{P} \times \mathbf{V}$, involved in (5b) should be carefully addressed. In fixed-point stabilization problem, $\boldsymbol{\Delta}_\Gamma$ converges to zero. However, $\boldsymbol{\Delta}_\Gamma$ should be estimated then used as an feedforward term for enhancing the control performance. Since the angular velocity can be measured at high frequency and with good precision, we propose to estimate $\boldsymbol{\Delta}_\Gamma$ using a high-gain observer similarly to the idea proposed in [5, Proposition 8].

Lemma 2 *Consider the following observer of $\boldsymbol{\Delta}_\Gamma$:*

$$\begin{cases} \mathbf{J}\dot{\hat{\boldsymbol{\Omega}}} = (\mathbf{J}\boldsymbol{\Omega}) \times \hat{\boldsymbol{\Omega}} + \boldsymbol{\Gamma}_c + \boldsymbol{\Gamma}_g + \hat{\boldsymbol{\Delta}}_\Gamma + k_0\mathbf{J}(\boldsymbol{\Omega} - \hat{\boldsymbol{\Omega}}) \\ \dot{\hat{\boldsymbol{\Delta}}}_\Gamma = a_0^2k_0^2\mathbf{J}(\boldsymbol{\Omega} - \hat{\boldsymbol{\Omega}}) \end{cases}$$

with $\hat{\boldsymbol{\Omega}}$ and $\hat{\boldsymbol{\Delta}}_\Gamma$ the estimates of $\boldsymbol{\Omega}$ and $\boldsymbol{\Delta}_\Gamma$, respectively; $\hat{\boldsymbol{\Omega}}(0) \in \mathbb{R}^3$, $\hat{\boldsymbol{\Delta}}_\Gamma(0) \in \mathbb{R}^3$; a_0, k_0 some positive gains. Assume that $\dot{\boldsymbol{\Delta}}_\Gamma$ is uniformly ultimately bounded (u.u.b.). Then for any $a_0 \in (1 - \sqrt{2}/2, 1 + \sqrt{2}/2)$,

1) *The errors $\hat{\boldsymbol{\Omega}} - \boldsymbol{\Omega}$ and $\hat{\boldsymbol{\Delta}}_\Gamma - \boldsymbol{\Delta}_\Gamma$ are u.u.b. by a positive constant $\varepsilon(k_0)$ that tends to zero when k_0 tends to $+\infty$. Moreover, these terms converge exponentially to zero for any $k_0 > 0$ if $\boldsymbol{\Delta}_\Gamma$ is constant.*
2) *$\dot{\hat{\boldsymbol{\Delta}}}_\Gamma$ is u.u.b. by a constant independent of k_0.*

The proof proceeds identically to the proof of [5, Proposition 8].

Define the angular velocity error variable $\tilde{\boldsymbol{\Omega}} \triangleq \boldsymbol{\Omega} - \boldsymbol{\Omega}_r$. From (5b), one obtains the following error equation

$$\mathbf{J}\dot{\tilde{\boldsymbol{\Omega}}} = (\mathbf{J}\boldsymbol{\Omega})_\times \tilde{\boldsymbol{\Omega}} + \boldsymbol{\Gamma}_c + \boldsymbol{\Gamma}_g + \boldsymbol{\Gamma} + \hat{\boldsymbol{\Delta}}_\Gamma + \bar{\boldsymbol{\Delta}}_\Gamma \tag{32}$$

with $\boldsymbol{\Gamma} \triangleq (\mathbf{J}\boldsymbol{\Omega})_\times \boldsymbol{\Omega}_r - \mathbf{J}\dot{\boldsymbol{\Omega}}_r$ and $\bar{\boldsymbol{\Delta}}_\Gamma \triangleq \boldsymbol{\Delta}_\Gamma - \hat{\boldsymbol{\Delta}}_\Gamma$.

Proposition 4 *(See [14] for the proof) Consider error equation given by (32). Introduce the following integrator*

$$\dot{\mathbf{z}}_\Omega = \tilde{\boldsymbol{\Omega}}, \;\; \mathbf{z}_\Omega(0) \in \mathbb{R}^3$$

Apply the control torque

$$\boldsymbol{\Gamma}_c = -\operatorname{sat}^{\eta_3}(\mathbf{K}_\Omega \tilde{\boldsymbol{\Omega}}) - \mathbf{K}_{i\Omega}\mathbf{z}_\Omega - \boldsymbol{\Gamma} - \hat{\boldsymbol{\Delta}}_\Gamma$$

with $\mathbf{K}_{i\Omega}, \mathbf{K}_\Omega \in \mathbb{R}^{3\times 3}$ positive diagonal gain matrices, η_3 a positive number, $\boldsymbol{\Omega}_r$ defined by (8) *combined with* (31)*, and with $\hat{\boldsymbol{\Delta}}_\Gamma$ given by Lemma 2. Assume that $\boldsymbol{\Delta}_\Gamma$ is constant. Then, the following properties hold.*

1) *The error state $(\tilde{\boldsymbol{\Omega}}, \mathbf{z}_\Omega, \mathbf{R}\mathbf{e}_3)$ converges either to $(\mathbf{0}, \mathbf{0}, \mathbf{e}_3)$ or $(\mathbf{0}, \mathbf{0}, -\mathbf{e}_3)$ for all initial conditions.*
2) *The equilibrium $(\tilde{\boldsymbol{\Omega}}, \mathbf{z}_\Omega, \mathbf{R}\mathbf{e}_3) = (\mathbf{0}, \mathbf{0}, \mathbf{e}_3)$ is almost-GAS and LES. The equilibrium $(\tilde{\boldsymbol{\Omega}}, \mathbf{z}_\Omega, \mathbf{R}\mathbf{e}_3) = (\mathbf{0}, \mathbf{0}, -\mathbf{e}_3)$ is unstable.*

V. Simulation results

The proposed control approach has been tested in simulation using a realistic model where the physical parameters are given in Tab. I.

The robustness of the proposed controller with respect to model uncertainties are tested by using the "erroneous" estimated parameters $\hat{\mathbf{J}}, \hat{\mathbf{M}}$ given by

$$\begin{cases} \hat{\mathbf{M}} = m\mathbf{I}_3 + \hat{\mathbf{M}}_a = \operatorname{diag}(17.868, 23.868, 21.024) \; [kg] \\ \hat{\mathbf{J}} = \hat{\mathbf{J}}_0 + \hat{\mathbf{J}}_a \quad = \operatorname{diag}(0.3105, 0.8486, 1.0) \; [kg.m^2] \end{cases}$$

Specification	Numerical value
$m\ [kg]$	16
$F_b\ [N]$	$1.01mg$
$l\ [m]$	0.025
$\mathbf{r}_C\ [m]$	$[0.2 \;\; 0 \;\; 0.1]$
$\mathbf{J}_0\ [kg.m^2]$	$\begin{bmatrix} 0.0842 & 0.004 & 0.005 \\ 0.004 & 0.2643 & 0.007 \\ 0.005 & 0.007 & 0.3116 \end{bmatrix}$
$\mathbf{J}_a\ [kg.m^2]$	$\begin{bmatrix} 0.1 & 0.005 & 0.006 \\ 0.005 & 0.25 & 0.008 \\ 0.006 & 0.008 & 0.3 \end{bmatrix}$
$\mathbf{M}_a\ [kg]$	$\begin{bmatrix} 1.39 & 0.10 & 0.12 \\ 0.10 & 4.26 & 0.13 \\ 0.12 & 0.13 & 4.02 \end{bmatrix}$
$\boldsymbol{\Xi} = ml\mathbf{e}_{3\times}[kg.m]$	$0.4\mathbf{e}_{3\times}$
$\mathbf{D}_{Vl}\ [kg.s^{-1}]$	$diag(5.85, 9.21, 11.03)$
$\mathbf{D}_{Vq}\ [kg.m^{-1}]$	$diag(36.57, 57.58, 68.97)$
$\mathbf{D}_{\Omega l}\ [kg.m^2.s^{-1}]$	$diag(0.01126, 0.01855, 0.01701)$
$\mathbf{D}_{\Omega q}\ [N.m]$	$diag(0.0053, 0.0130, 0.0118)$

TABLE I

Specifications of the simulated AUV

The homography $\mathbf{H}$ is directly computed using (6) with $d^\star = 1(m)$ and $\mathbf{n}^\star = [0.8259, 0.5364, -0.1736]^\top$ corresponding to $(\alpha^\star, \beta^\star) = (10°, 33°)$. The initial conditions are chosen as follows: $\boldsymbol{\xi}_C(0) = [-1, -0.5, -0.5]^\top(m)$, $\mathbf{R}(0) = \mathbf{R}_{\{\text{roll}=10°,\, \text{pitch}=-10°,\, \text{yaw}=45°\}}$, $\mathbf{V}(0) = \boldsymbol{\Omega}(0) = \mathbf{0}$. The initial yaw and camera's position are chosen rather large to verify the large stability domain of the proposed controller. Control parameters and gains[2] are summarized in Table II.

Controller	Gains and other parameters
Proposition 1	$k_{13} = 3s_1,\, k_{23} = \frac{8}{3}\frac{s_1^2}{n_1},\;\; k_{33} = 3\frac{s_1^2}{n_1},\;\; s_1 = 1$
Proposition 2	$k_1 = 3s_2,\, k_2 = \frac{8}{3}\frac{s_2^2}{n_1},\;\; k_3 = 3\frac{s_2^2}{n_1},\;\; s_2 = 1.1$
Proposition 3	$k_g = 1,\;\; k_{\Theta 1} = 0.0625,\;\; k_{\Theta 2} = 0.5,\;\; \Delta_\Theta = 1$
Proposition 4	$\mathbf{K}_{\boldsymbol{\Omega}} = 3\hat{\mathbf{J}},\;\; \mathbf{K}_{i\boldsymbol{\Omega}} = 0$ $a_0 = 0.5,\;\; k_0 = 20,\;\; \eta_3 = 8$

TABLE II

Control gains and parameters

The performance of proposed controller is illustrated by Figs. 5–8. One observes from Fig. 5 a smooth convergence to zero of the position and orientation errors. Fig. 6 shows the fast convergence to zero of the visual error $(\boldsymbol{\sigma}, \varrho)$ and their augmented variables $(\hat{\boldsymbol{\sigma}}, \hat{\varrho})$. The time evolutions of the control force and torque are shown in Fig. 7. All components of the control force and torque converge to zero except the third component of the control force that allows for compensating for $\mathbf{F}_{gb}$. The convergence of the angular velocity $\boldsymbol{\Omega}$ to the reference value $\boldsymbol{\Omega}_r$ as depicted in Fig. 8 shows the effectiveness of the inner-loop controller.

VI. Conclusion

In this paper a homography-based dynamic control approach of fully-actuated underwater vehicles equipped with a forward-looking camera observing a (near) vertical visual target is proposed. Since linear velocity measurements and homography decomposition are not required, the approach is appealing for low-cost applications. Improving the robustness of the outer-loop control to the external perturbations (e.g. current) is a topic our future work. Then a testing campaign with a real AUV will follow to validate the proposed approach in challenging sea environment.

References

[1] S. Benhimane and E. Malis. Homography-based 2d visual tracking and servoing. *Int. J. of Robotics Research*, 26(7):661–676, 2007.

[2] L. Brignone, M. Perrier, and C. Viala. A fully autonomous docking strategy for intervention AUVs. In *MTS/IEEE OCEANS'07*, pages 1–6, 2007.

[3] F. Chaumette and S. Hutchinson. Visual servo control, Part II: Advanced approaches. *IEEE Robotics and Automation Mag.*, 14(1):109–118, 2007.

[4] H. de Plinval, P. Morin, and P. Mouyon. Stabilization of a class of underactuated vehicles with uncertain position measurements and application to visual servoing. *Automatica, Elsevier*, 77(0):155–169, 2017.

[5] M.-D. Hua. *Contributions to the automatic control of aerial vehicles*. PhD thesis, 2009.

[6] M.-D. Hua, G. Allibert, S. Krupínski, and T. Hamel. Homography-based visual servoing for autonomous underwater vehicles. In *IFAC World Congress*, pages 5729–5733, 2014.

[7] H. K. Khalil. *Nonlinear systems (3rd Edition)*. Prentice Hall, 2002.

[8] S. Krupínski, G. Allibert, M.-D. Hua, and T. Hamel. An inertial-aided homography-based visual servoing control approach for (almost) fully actuated autonomous underwater vehicles. *IEEE Transactions on Robotics*, 33(5):1041–1060, 2017.

[9] N. E. Leonard. Stability of a bottom-heavy underwater vehicle. *Automatica*, 33(3):331–246, 1997.

[2]Tuned by applying the classical pole placement technique when considering $\mathbf{n} \equiv \mathbf{e}_1$.

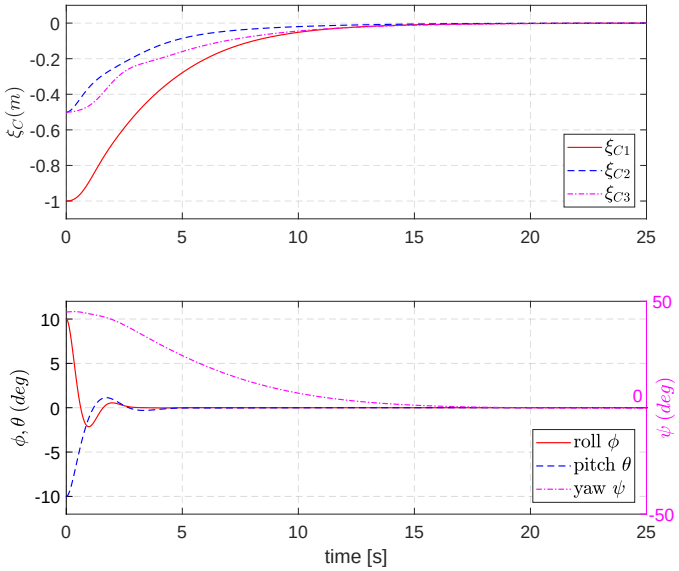

Fig. 5. AUV's position and attitude (Euler angles) vs. time

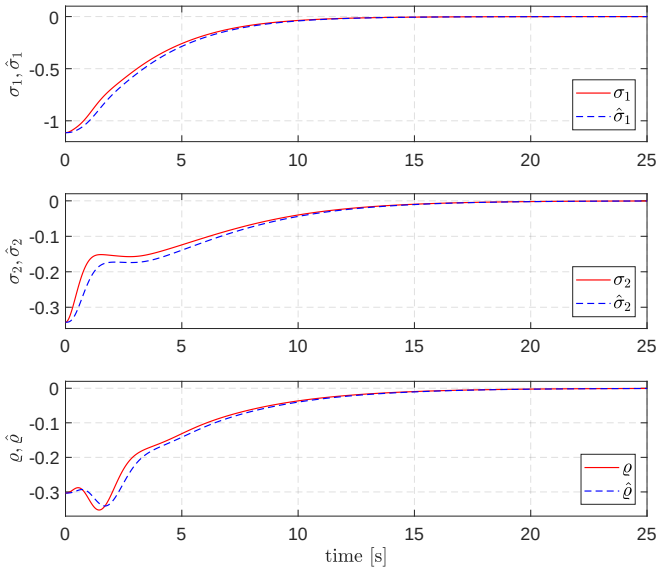

Fig. 6. Visual errors vs. time

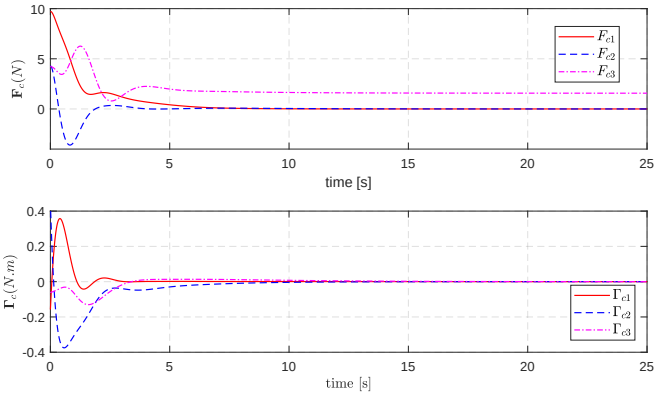

Fig. 7. Control force $\mathbf{F}_c$ and moment $\mathbf{\Gamma}_c$ vs. time

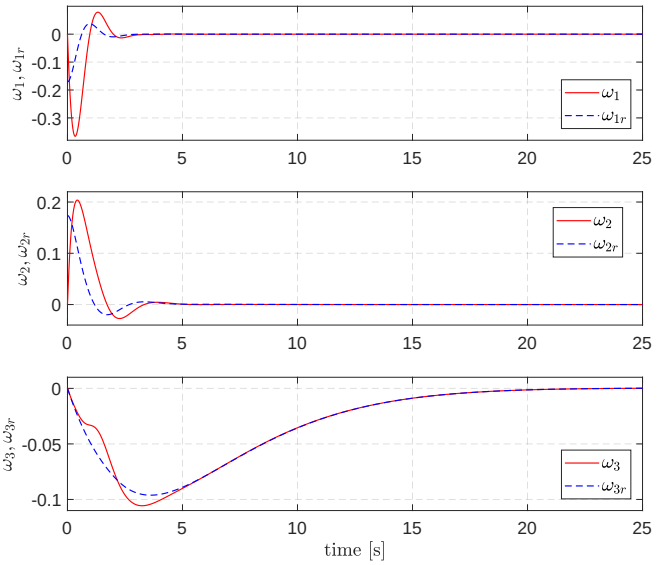

Fig. 8. $\mathbf{\Omega}$ and $\mathbf{\Omega}_r$ vs. time

[10] J.-E Lots, D. M. Lane, E. Trucco, and F. Chaumette. A 2-D visual servoing for underwater vehicle station keeping. In *IEEE Int. Conf. on Robotics and Automation (ICRA)*, pages 2767–2772, 2001.

[11] E. Malis, F. Chaumette, and S. Boudet. 2 1/2D visual servoing. *IEEE Trans. on Robotics and Automation*, 15(2):238–250, 1999.

[12] E. Malis and M. Vargas. Deeper understanding of the homography decomposition for vision-based control. *INRIA Research report*, RR-6303:90, 2007.

[13] F. Mufti, R. Mahony, and J. Kim. Super resolution of speed signs in video sequences. In *Digital Image Computing: Techniques and Applications (DICTA)*, pages 278–285, 2007.

[14] L.-H. Nguyen, M.-D. Hua, G. Allibert, and T. Hamel. Inertial-aided homography-based visual servo control of autonomous underwater vehicles without linear velocity measurements. In *21st International Conference on System Theory, Control and Computing (ICSTCC)*, pages 9–16, 2017.

[15] O. Saurer, P. Vasseur, R. Boutteau, C. Demonceaux, M. Pollefeys, and F. Fraundorfer. Homography based egomotion estimation with a common direction. *IEEE Transactions on Pattern Analysis and Machine Intelligence*, 39(2):327–341, 2017.

[16] D. Scaramuzza and R. Siegwart. Appearance-guided monocular omnidirectional visual odometry for outdoor ground vehicles. *IEEE Transactions on Robotics*, 24(5):1015–1026, 2008.

[17] S. van der Zwaan, A. Bernardino, and J. Santos-Victor. Visual station keeping for floating robots in unstructured environments. *Robotics and Autonomous Systems*, 39(3):145–155, 2002.

APPENDIX I
PROOF OF LEMMA 1

One verifies that $\mathbf{A}$ is Hurwitz if $k_3 > k_2 > 0$ by applying Routh-Hurwitz criterion on its characteristic polynomial $P_{\mathbf{A}}(\lambda) = \left(\lambda^3 + k_1\lambda^2 + n_1 k_3 \lambda + n_1(k_3 - k_2)k_1\right)^2$.

Consider the following positive diagonal matrix

$$\mathbf{Q} = \begin{bmatrix} q\mathbf{I}_2 & 0 & 0 \\ 0 & q\mathbf{I}_2 & 0 \\ 0 & 0 & \bar{\mathbf{M}}^{-2} \end{bmatrix}, \quad q > 0$$

According to the Lyapunov theorem [7], there exists a unique $\mathbf{D} = \mathbf{D}^\top > 0$ such that $\mathbf{DA} + \mathbf{A}^\top\mathbf{D} = -\mathbf{Q}$. Straightforward computations result in

$$\mathbf{D} = \frac{1}{2}\begin{bmatrix} d_{11}\mathbf{I}_2 & d_{12}\mathbf{I}_2 & d_{13}\bar{\mathbf{M}}^{-1} \\ d_{12}\mathbf{I}_2 & d_{22}\mathbf{I}_2 & d_{23}\bar{\mathbf{M}}^{-1} \\ d_{13}\bar{\mathbf{M}}^{-1} & d_{23}\bar{\mathbf{M}}^{-1} & d_{33}\bar{\mathbf{M}}^{-2} \end{bmatrix} \tag{33}$$

with

$$\begin{array}{l} d_{11} \triangleq \frac{1}{k_1}\left(\frac{k_2}{n_1}+\frac{k_3+k_2}{k_3-k_2}q\right) \\ d_{12} \triangleq -\frac{1}{k_1}\left(\frac{k_3}{n_1}+q\right) \\ d_{13} \triangleq \frac{1}{n_1}+\frac{2q}{k_3-k_2} \\ d_{22} \triangleq \frac{k_1}{n_1}\left(\frac{k_3}{k_2}-1\right)\left(\frac{1}{n_1}+\frac{2q}{k_3-k_2}\right)+\frac{k_3}{k_1k_2}\left(\frac{k_3}{n_1}+q\right) \\ d_{23} \triangleq -\frac{1}{n_1} \\ d_{33} \triangleq \frac{n_1}{k_1k_2}\left(\frac{k_3}{n_1}+q\right)+\frac{k_1}{k_2}\left(\frac{1}{n_1}+\frac{2q}{k_3-k_2}\right) \end{array} \tag{34}$$

Consider the Lyapunov function $\mathcal{L}_1 \triangleq \mathbf{X}^\top\mathbf{D}\mathbf{X}$, with $\mathbf{D}$ given by (33)–(34). After some straightforward computations, one deduces

$$\begin{array}{l} \dot{\mathcal{L}}_1 = \mathbf{X}^\top(\mathbf{D}\mathbf{A}+\mathbf{A}^\top\mathbf{D})\mathbf{X}+\mathbf{X}^\top(\mathbf{D}\mathbf{B}+\mathbf{B}^\top\mathbf{D})\mathbf{X} \\ = -\left(\frac{x_{31}^2}{m_1^2}+\frac{x_{32}^2}{m_2^2}\right)\left[1-\frac{n_2^2}{4q}\left(d_{12}^2+d_{22}^2\right)\right] \\ -\left(\sqrt{q}x_{11}+\frac{d_{12}n_2}{2\sqrt{q}m_2}x_{32}\right)^2-\left(\sqrt{q}x_{12}-\frac{d_{12}n_2}{2\sqrt{q}m_1}x_{31}\right)^2 \\ -\left(\sqrt{q}x_{21}+\frac{d_{22}n_2}{2\sqrt{q}m_2}x_{32}\right)^2-\left(\sqrt{q}x_{22}-\frac{d_{22}n_2}{2\sqrt{q}m_1}x_{31}\right)^2 \end{array} \tag{35}$$

Now the task consists in finding sufficient conditions for (k_1,k_2,k_3,q) so that

$$1 > \frac{n_2^2}{4q}\left(d_{12}^2+d_{22}^2\right) \tag{36}$$

which ensures that $\dot{\mathcal{L}}$ is negative definite and, thus, the origin of System (27) is GAS. Note that d_{12} and d_{22} are functions of (k_1,k_2,k_3,q) as defined in (34).

From (7) and (28), one verifies that $\frac{n_1^2}{n_2^2} > 1+\sqrt{2}$. Define $\delta \triangleq \frac{n_1^2}{n_2^2}-(1+\sqrt{2})>0$. One verifies that $\delta = \frac{1}{\arctan^2\beta^\star} - \frac{1}{\arctan^2\beta^\star_{max}}$. Rewrite $k_3=\gamma k_2$ (with $\gamma>1$) and $k_1=\alpha k_2$ (with $\alpha>0$). Denote

$$\zeta_1 \triangleq \frac{\alpha(\gamma-1)k_2}{n_1^2}\frac{\alpha n_1}{\gamma^2},\ \zeta_2 \triangleq \frac{n_1\gamma}{\alpha^2k_2},\ \bar{\zeta} \triangleq \zeta_2(1-\zeta_1\zeta_2)$$

After some computations, one verifies that inequality (36) is equivalent to

$$\begin{array}{l} \alpha^2\left[\bar{\zeta}^2+(2+\zeta_2)^2\right]q^2+\frac{1}{\alpha^2}\left[\frac{1}{(1-\zeta_1\zeta_2)^2}+\frac{(\zeta_1+1)^2}{(1-\zeta_1\zeta_2)^4}\right] \\ +2\left[\zeta_2+\frac{(\zeta_1+1)(\zeta_2+2)}{(1-\zeta_1\zeta_2)^2}-2-2\sqrt{2}-2\delta\right]q<0 \end{array} \tag{37}$$

Denote

$$\begin{array}{l} \boldsymbol{\zeta} \triangleq \left[\begin{array}{cc}\zeta_1 & \zeta_2\end{array}\right]^\top,\ \ g_1(\boldsymbol{\zeta}) \triangleq \zeta_2+\frac{(\zeta_1+1)(\zeta_2+2)}{(1-\zeta_1\zeta_2)^2} \\ g_2(\boldsymbol{\zeta}) \triangleq \left[\zeta_2^2+\frac{(2+\zeta_2)^2}{(1-\zeta_1\zeta_2)^2}\right]\left[1+\frac{(\zeta_1+1)^2}{(1-\zeta_1\zeta_2)^2}\right] \end{array}$$

The condition for inequality (37) having solution $q>0$ is

$$\left\{\begin{array}{l} \Delta' = \left(g_1(\boldsymbol{\zeta})-2-2\sqrt{2}-2\delta\right)^2-g_2(\boldsymbol{\zeta})>0 \\ -\left(g_1(\boldsymbol{\zeta})-2-2\sqrt{2}-2\delta\right)>0 \end{array}\right.$$

or equivalently

$$\delta > g(\boldsymbol{\zeta}) \triangleq \frac{g_1(\boldsymbol{\zeta})-2}{2}+\frac{\sqrt{g_2(\boldsymbol{\zeta})}-2\sqrt{2}}{2} \tag{38}$$

We will show that we can always choose positive control gains k_1,k_2,k_3 (i.e. ζ_1,ζ_2) such that condition (38) holds. One verifies that $g_1(\boldsymbol{\zeta})>2$, $g_2(\boldsymbol{\zeta})>8$, $g(\boldsymbol{\zeta})>0$, with $\zeta_1,\zeta_2>0$. One also has

$$\lim_{\zeta_1,\zeta_2\to 0^+} g_1(\boldsymbol{\zeta}) = 2,\quad \lim_{\zeta_1,\zeta_2\to 0^+} g_2(\boldsymbol{\zeta}) = 8$$

and consequently

$$\lim_{\zeta_1,\zeta_2\to 0^+} g(\boldsymbol{\zeta}) = 0 \tag{39}$$

From (39), with $g(\boldsymbol{\zeta})$ defined in (38), one deduces that $\forall\delta>0$ there exists $\zeta^*>0$ such that $g(\boldsymbol{\zeta})<\delta$ whenever $|\boldsymbol{\zeta}|<\zeta^*$. This implies that there always exist $\zeta_1=\frac{n_1k_3}{k_1^2}$ and $\zeta_2=\left(1-\frac{k_2}{k_3}\right)\frac{1}{\zeta_1}$ small enough such that $\sqrt{\zeta_1^2+\zeta_2^2}<\zeta^*$ and, consequently, (36) is satisfied. Therefore, there exist $\bar{k}_1>0$ large and $\epsilon>0$ small enough such that inequality (36) has solution $q>0$ provided that $k_1>\bar{k}_1$, $1<\frac{k_3}{k_2}<1+\epsilon$.

Appendix II
Proof of Proposition 2

In view of the singular perturbation theory [7] it suffices to prove that the origin of the nominal system

$$\dot{\mathbf{X}} = -\omega_{3r}(t)\bar{\mathbf{S}}\mathbf{X}+\mathbf{A}\mathbf{X}+\mathbf{B}\mathbf{X}-\tilde{\omega}_3\bar{\mathbf{S}}\mathbf{X} \tag{40}$$

is (globally) exponentially stable. As a consequence of Lemma 1, there exists $\nu>0$ such that

$$\mathbf{X}^\top(\mathbf{A}^\top\mathbf{D}+\mathbf{D}\mathbf{A}+\mathbf{B}^\top\mathbf{D}+\mathbf{D}\mathbf{B})\mathbf{X} \le -\nu|\mathbf{X}|^2$$

Since $\tilde{\omega}_3$ converges to zero, for any $0<\varepsilon_\omega<1$ there exists $T>0$ such that $\forall\tau\ge T$, $|\tilde{\omega}_3(\tau)|\le\frac{\varepsilon_\omega\nu}{2\|\mathbf{D}\|}$ and, subsequently,

$$\dot{\mathcal{L}}_1(\tau\ge T) \le -(1-\varepsilon_\omega)\nu|\mathbf{X}|^2+2(\sup|\omega_{3r}|)\|\mathbf{D}\||\mathbf{X}|^2$$

If $\sup|\omega_{3r}|<\varpi\triangleq\frac{1-\varepsilon_\omega}{2\|\mathbf{D}\|}\nu$, there exists $\nu_1>0$ such that $\dot{\mathcal{L}}_1(\tau\ge T)\le-\nu_1\mathcal{L}_1(\tau\ge T)$, implying the exponential convergence of $\mathbf{X}$ to zero.